A Fast Mesh Deformation Method for Neuroanatomical Surface Inflated Representations

Andrea Rueda[1], Álvaro Perea[2], Daniel Rodríguez-Pérez[2], and Eduardo Romero[1]

[1] BioIngenium Research Group, Universidad Nacional de Colombia, Carrera 30 45-03, Bogotá, Colombia
{adruedao,edromero}@unal.edu.co
[2] Department of Mathematical Physics and Fluids, Universidad Nacional de Educación a Distancia, c/ Senda del Rey, 9, 28040 Madrid, Spain
{aperea,daniel}@dfmf.uned.es

Abstract. In this paper we present a new metric preserving deformation method which permits to generate smoothed representations of neuroanatomical structures. These surfaces are approximated by triangulated meshes which are evolved using an external velocity field, modified by a local curvature dependent contribution. This motion conserves local metric properties since the external force is modified by explicitely including an area preserving term into the motion equation. We show its applicability by computing inflated representations from real neuroanatomical data and obtaining smoothed surfaces whose local area distortion is less than a 5 %, when comparing with the original ones.

Keywords: area-preserving deformation model, deformable geometry, surface inflating.

1 Introduction

Computational technologies have recently invaded medical practice, changing in many ways clinical activities and becoming an important tool for patient diagnosis, treatment and follow-up. In particular, the use of three-dimensional models, obtained from medical images such as Magnetic Resonance, Positron Emission Tomography or Computed Tomography, improves visualization and functional analysis of anatomical structures with intricate geometry. Morphometrical studies require a high degree of precision and reproducibility [1], tasks which are difficult to achieve because of the complexity of such structures. Assessment of lengths and areas on these surfaces is a very high time-consuming process, a factor which limits large anatomical studies. This problematic situation is worsen when one considers that morphometrical studies show variabilities which can reach a 30 % [1], an unacceptable figure for many investigations. This

D. Mery and L. Rueda (Eds.): PSIVT 2007, LNCS 4872, pp. 75–86, 2007.

kind of procedures can be improved by assistance of recent semi-automated or full-automated developed techniques, but they are generally addressed to measure deep brain structures through voxel-based [2] or object-based [3] strategies. Lately, a deformation of the original surface into a simpler one turns out to overcome most of these difficulties since measurements can be carried out on simpler and smoother surfaces [4, 5]. These morphometric tasks may thus be simplified if lengths and areas are calculated over topologically equivalent, smoother versions of the surface, subjected to the condition that the metric properties must be appropriately preserved.

Deformable models, those where a 2D contour or a 3D surface evolves towards a target contour or surface, have been extensively studied during the last 20 years. 2D deformable models were introduced by Kass et al. [6] and extended to 3D applications by Terzopoulos et al. [7]. A broad range of applications of these models includes pattern recognition, computer animation, geometric modeling, simulation and image segmentation, among others [8]. A number of previous works [9, 10, 11, 12, 13, 14, 15, 16, 17, 18, 19, 20] have focused on application of deformable models to cerebral cortex analysis. In these papers, several models are able to generate different types of smoothed representations. These works introduce different surface-based analyses of the cerebral cortex, such as surface smoothing, geometric transformations, projections or mappings, surface flattening and other types of deformations.

Recent work in surface deformation has been addressed to generate three types of representations: unfolded, inflated, and spherical. Unfolding methods transform the original 3D surface into a planar representation, which sometimes require inserting cutting paths onto the surface boundary, a simple strategy which permits to reduce the stretch of the flattened surface. Surface smoothing methods iteratively inflate the surface, retaining its overall shape and simplifying its geometry. Spherical or ellipsoidal representations can be obtained by defining a conformal mapping from the original surface onto a sphere or ellipsoid. These representations generally attempt to facilitate visualization of a particular structure, disregarding metric preserving restrictions.

Concerning surface deformation methods under the restriction of metric preservation, a lot of work has been dedicated to build conformal or quasi-conformal mappings of the brain surface. These approaches use an important theorem from the Riemannian geometry, namely, that a surface of genus zero (without any handles, holes or self-intersections) can be conformally mapped onto a sphere and any local portion thereof onto a disk. Conformal mappings are angle preserving and many attempts have been made at designing also quasi-length or area-preserving mappings [21, 22, 23, 24, 25, 26], reporting metric distortions close to 30 % of the original surface. On the other hand, different methods propose a set of local forces, which guarantees an approximated metric preservation[1] while smoothing the surface [19, 22, 27, 28]. It is well known that it is impossible to exactly preserve distances, or to preserve angles and areas simultaneously because the original surface and its smoothed version will have

[1] These methods report metric distortions up to a 20 % of the original surface.

different Gaussian curvature [29]. Pons et al. [30] presented a method to deform the cortical surface while area distortion is less than a 5 %. The whole approach uses a tangential motion which depends on the normal motion, constructed for ensuring area preservation. However, implementation is performed using high computational cost representations such as level sets [31].

Our main goal was to develop an efficient and accurate deformation method constrained by tough area preservation conditions for mesh representations. In the present work a novel formulation, meeting the requirement of area preservation for evolving surfaces, is introduced. The original surface, approximated by a triangulated mesh, is modified by applying an external velocity field, which iteratively drives the surface towards a desired geometrical configuration. This velocity field is composed of a smoothness force, used to move each point in the surface towards the centroid of its neighbors and a radial expansion term. This last term combines a radial velocity (such as the distance to a desired sphere surface) and a geometrical component which depends on the local curvature and is charged of maintaining local area properties.

This paper is organized as follows. Section 2 describes the proposed method, giving details related to the local area preservation condition and to the deformation process. Results obtained by applying the deformation method to phantom and actual surfaces are presented in Section 3 and conclusions in Section 4.

2 Methods and Models

In this section we develop the mathematical model which includes conditions for the preservation of local area of an evolving surface, represented by a triangulated mesh. We then introduce the smoothing and radial expansion terms, which guide the deformation process. Finally we describe the complete velocity model, together with a description of the surface evolution algorithm.

2.1 Local Area Preservation

The whole approach can be formulated as follows: consider a surface which is represented by a triangulated mesh, composed of N nodes. This mesh is forced to deform into a desired surface subjected to the condition that the local Euclidean metric must be preserved. Let us define the total area $S\left(\{\mathbf{x}_i\}_{i=1}^N\right)$ as a function of the node coordinates $\mathbf{x}_i$, while the global conservation condition of S upon motion of the $\mathbf{x}_i$, parameterized as $\mathbf{x}_i(t)$, is

$$\sum_{i=1}^{N} \dot{\mathbf{x}}_i \cdot \frac{\partial}{\partial \mathbf{x}_i} S\left(\{\mathbf{x}_k\}_{k=1}^N\right) = 0 \tag{1}$$

where the $\dot{\mathbf{x}}_i$ denotes the derivative of $\mathbf{x}_i$ with respect to the parameter t (that we will refer to as time).

The total area S, written as the sum of the mesh triangle areas, can be decomposed for a given node of coordinates $\mathbf{x}_i$ as

$$S = \sum_l s_l^i + S_i'$$

where the s_l^i represents the area of all the triangles having $\mathbf{x}_i$ as one of their vertices, and S_i' stands for the area of the rest of the triangles, none of which has $\mathbf{x}_i$ as a vertex.

Thus, we can rewrite (1) on a per vertex basis as

$$\sum_{i=1}^{N} \dot{\mathbf{x}}_i \cdot \frac{\partial}{\partial \mathbf{x}_i} \sum_l s_l^i = 0$$

so that a convenient solution to this equation is

$$\dot{\mathbf{x}}_i \cdot \frac{\partial}{\partial \mathbf{x}_i} \sum_l s_l^i = 0 \tag{2}$$

which clearly fulfills the searched condition.

Let us then define from expression (2) a vector

$$\kappa_i = \frac{\partial}{\partial \mathbf{x}_i} \sum_l s_l^i$$

which can be seen as a "curvature vector" associated to the i-th vertex so that local area preservation is guaranteed when the variation of $\mathbf{x}_i$ is perpendicular to κ_i. This local estimation of the curvature κ_i is a vector for each mesh point, expressed as

$$\kappa_i = \sum_{j \in N_i} |x_j - x_{j+1}| \frac{\mathbf{a} - \mathbf{b}\cos\alpha}{2\sin\alpha}$$

where N_i is the set of vertices neighboring the i-th vertex, $\mathbf{a} = \frac{x_i - x_j}{|x_i - x_j|}$ and $\mathbf{b} = \frac{x_j - x_{j+1}}{|x_j - x_{j+1}|}$ are unit vectors with directions defined in the triangle with vertices i, j and $j+1$, and α is the angle between them which satisfies $\mathbf{a} \cdot \mathbf{b} = \cos\alpha$.

2.2 Smoothing Terms

The local smoothing term $f_{SL}(i)$ is calculated for each point $\mathbf{x}_i$ as the difference between the center of mass $\mathbf{x}_{CM}$ of the triangles that share the vertex $\mathbf{x}_i$ and the position of this vertex, that is to say

$$f_{SL}(i) = \mathbf{x}_{CM}(i) - \mathbf{x}_i, \text{ where } \mathbf{x}_{CM}(i) = \frac{1}{N_i} \sum_{j \in N_i} \mathbf{x}_j \ .$$

On the other hand, a global smoothing term is calculated as

$$f_{SG} = \frac{1}{N} \sum_{i}^{N} \sum_{j \in N_i} \mathbf{n}_i \cdot (\mathbf{x}_i - \mathbf{x}_j)\mathbf{n}_i$$

where $\mathbf{n}_i$ is the average normal vector on every triangle which shares the i-th vertex and the sum on j is on all neighbors of the i-th vertex. The total smoothing term $f_S(i) = f_{SL}(i) + f_{SG}$, proposed by Fischl et al. [20], drives each vertex in the direction of the centroid of its neighbors.

2.3 Radial Expansion Motion

Overall, the expansion movement is imposed by three different components: a radial velocity which is defined by the user, a geometrical component which depends on the local curvature and a radial expansion which forces the surface towards a hypothetical sphere. All these forces point out to a direction on the average normal $\mathbf{n}_i$ of the i-th vertex, as follows

$$h_R(i) = [\mathbf{v}_{\text{radial}}(i) + F(\kappa_i) + (R_{\text{ext}} - \mathbf{x}_i \cdot \mathbf{n}_i)]\,\mathbf{n}_i$$

where $F(\kappa_i)) = -\kappa_i$, so that if the curvature is positive (belly shape), the surface is flattened towards the interior and when the curvature is negative (hole shape) the surface is flattened towards the exterior. The reference value R_{ext} corresponds to the maximum distance between the whole surface and its center of mass. This term forces out the points towards the circumscribed sphere.

2.4 Velocity Model

Let us now assume that we impose a deformation field such that every vertex $\mathbf{x}_i$ is moving with a particular "velocity" $\mathbf{v}(\mathbf{x}_i)$, which is dependent on the vertex position. Then, the evolution equation for each point is

$$\dot{\mathbf{x}}_i = f_{SL}(i) + f_{SG} + \lambda_i h_R(i)$$

where λ_i is a local parameter which takes into account the relative weight of the radial expansion and smoothing. Such weight function is estimated from the local conservation relationship $\dot{\mathbf{x}}_i \cdot \kappa_i = 0$ so that

$$\lambda_i = -\frac{\kappa_i \cdot (f_{SL}(i) + f_{SG})}{\kappa_i \cdot h_R(i)}\ . \tag{3}$$

In order to prevent stiffness phenomena during the surface evolution, an additional parameter β is introduced into the expansion term

$$\dot{\mathbf{x}}_i = f_{SL}(i) + f_{SG} + [(1+\beta)\lambda_i - \beta\lambda]h_R(i) \tag{4}$$

also, a global weight function λ is included

$$\lambda = -\frac{\sum_i \kappa_i \cdot (f_{SL}(i) + f_{SG})}{\sum_i \kappa_i \cdot h_R(i)}\ .$$

This evolution equation combines, in an arithmetic proportion, local and global preservation effects; which is the constrained motion model used in this paper.

2.5 Surface Evolution Process

This external velocity field imposes an expansion or contraction movement driven by the radial force. Physically, this amounts to an internal pressure which acts on a smoothed surface, result of a re-distribution effect of the surface tension

caused by the pressure changes. The radial expansion movement is then a consequence of the resultant pressure excess. According to this scheme, a two-phase surface evolution process is proposed. In the first stage, only the local and global smoothing terms are applied, updating the mesh position points. Once the surface is smoothed, the radial expansion factor which includes the local preservation term, is calculated and applied to the point coordinates of the smoothed surface. Algorithm 1 summarize the whole process and is hereafter presented.

Algorithm 1. Surface Evolution

Set the time step dt and the β parameter
repeat
  Calculate the global smoothing force f_{SG}
  for $i = 1$ to N **do**
    Calculate the local smoothing force $f_{SL}(i)$
    Update the point coordinates $\tilde{\mathbf{x}}_i(t) = \mathbf{x}_i(t) + [f_{SL}(i) + f_{SG}]dt$
  end for
  for $i = 1$ to N **do**
    Calculate the radial expansion force $h_R(i)$
    Calculate the local weighting parameter λ_i
  end for
  Calculate the global weighting parameter λ
  for $i = 1$ to N **do**
    Update the point coordinates $\mathbf{x}_i(t + dt) = \tilde{\mathbf{x}}_i(t) + [(1 + \beta)\lambda_i - \beta\lambda]h_R(i)dt$
  end for
until Some convergence criterion is met

3 Results and Discussion

In this section we compute inflated representations from both phantom and actual neuroanatomical data. Then, a description of the actual surfaces is introduced together with implementation and evaluation issues.

3.1 Phantoms

At a first stage, the deformation model was evaluated over phantom surfaces, generated and modified using a Mathematica™ routine (version 5.0), which implements the surface evolution process presented in Algorithm 1. These surfaces were obtained by mixing up simple shapes as illustrated in Figure 1, with similar discontinuities to the actual neuroanatomical data. The number of triangles varied between 192 and 288 and the area units were defined for each surface from the isotropical cartesian space generated for each case. Figure 1 illustrates our technique with a phantom surface, constructed via two spheres which results in a single discontinuity. The initial surface is displayed at the left panel and the resultant surface, after 25 iterations, at the right panel. In this example, the total area of both surfaces is $20,95$ area units so the total area was

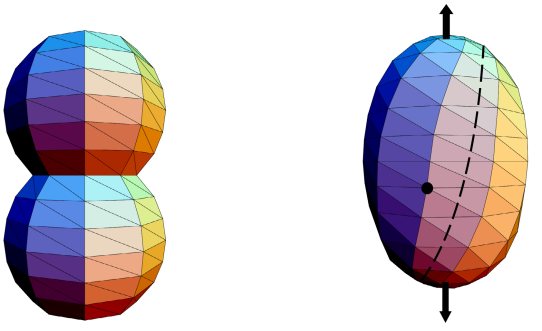

Fig. 1. Result of applying our deformation model on a phantom image. (a) Initial surface. (b) Deformed surface.

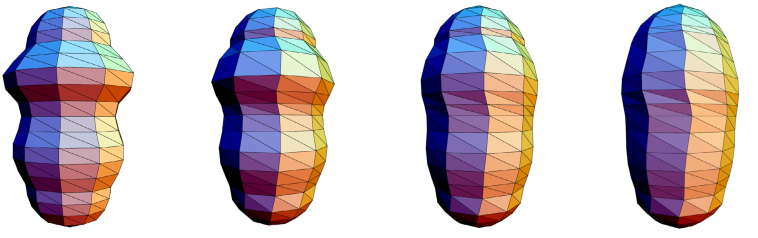

Fig. 2. Result of applying our deformation model, using a different β, on a phantom image. (a) Initial surface. (b) With $\beta = 0.5$. (c) With $\beta = 1.0$. (d) With $\beta = 1.5$.

preserved. Note that the smooth force, subjected to the preservation condition, redistributes point positions, an effect which can be here observed as a twist of the main surface direction.

Figure 2 shows, upon a phantom surface similar to a brain stem, how the model was proved using different values of the β parameter. Figure 2 presents the initial surface (panel 2(a)) and results obtained with β values of 0.5, 1.0 and 1.5 are shown at panels 2(b), 2(c) and 2(d), respectively. After 10 iterations and a set time step of $dt = 0.1$, the three resulting surfaces presents variable degrees of deformation, without any metric distortion.

3.2 Real Surfaces

Performance of the surface evolution process was also assessed on 3D surfaces, obtained from actual neuroanatomical data. The whole implementation was written in C++, using the VTK (www.vtk.org) functions for interaction and visualization of these structures. All these routines run on a Linux system with a 2.13 GHz Intel Core 2 Duo processor and 2GB in RAM memory.

Datasets. Brain stem and cerebellum triangulated surfaces, segmented and reconstructed from medical images were used as input of the algorithm. The former was obtained from a $512 \times 512 \times 50$ computed tomographic image and the resulting mesh was composed of 2800 points and 5596 triangles, while the latter was obtained from a $512 \times 512 \times 40$ computed tomographic image which resulted in a mesh composed of 4650 points and 9296 triangles.

Implementation Issues. The simple over-relaxation scheme proposed in Equation 4 for integration, was replaced by a one step predictor-corrector scheme [32]. The local preserving condition is introduced through a λ_i parameter which obliges the curvature vector κ_i to be perpendicular to the direction of the smoothing force. Denominator of the λ_i parameter (see Equation 3) was forced to be larger than 0.001 for avoiding discontinuities. A global area preservation factor λ facilitates a proper handling of the general preserving contribution while relaxes the local conservation condition. A β parameter is also introduced for managing the balance between local and global contributions (see Equation 4). All the examples use a β parameter set at 0.2 and $dt = 0.001$. Finally, the total smoothness force was also weighted using a factor set to 1.2 in the same equation.

Evaluation Issues. For evaluation purposes a local area factor J_i at point $\mathbf{x}_i$ of the surface is introduced as $J_i = A^0_{p_i}/A^t_{p_i}$, where $A^0_{p_i}$ is the initial area and $A^t_{p_i}$ is the current area of the patch around this point, defined by the area of the triangles which share the point $\mathbf{x}_i$. A decreasing J_i indicates a local area

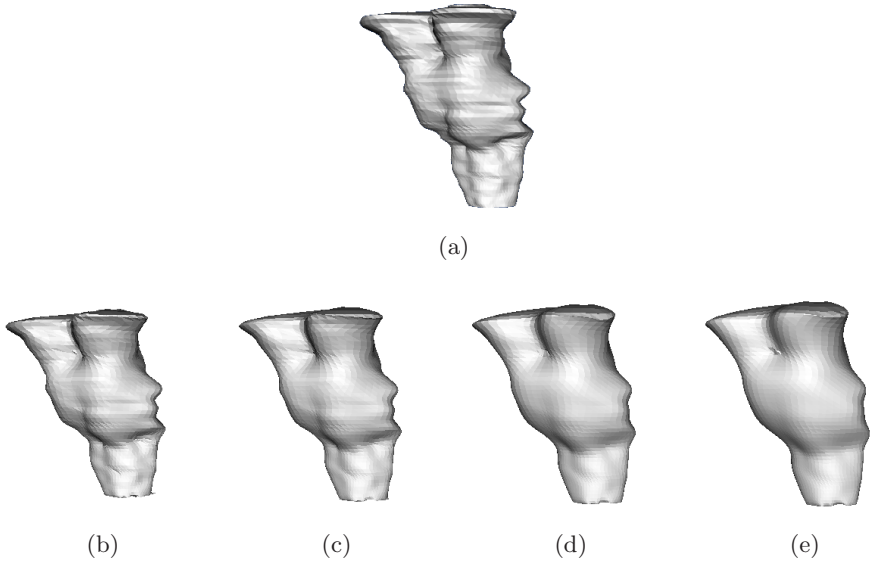

Fig. 3. Result of applying our deformation model on a brain stem surface. (a) Initial surface. (b) Iteration 500. (c) Iteration 1000. (d) Iteration 2000. (e) Iteration 3000.

Table 1. Normalized area factor $J/\bar{J}$ for the brain stem surface

$J/\bar{J}$	Number of patches	% of patches
$0.0 - 0.75$	0	0 %
$0.76 - 0.95$	0	0 %
$0.96 - 1.04$	2722	97.21 %
$1.05 - 1.24$	71	2.54 %
$1.25 - 2.0$	7	0.25 %

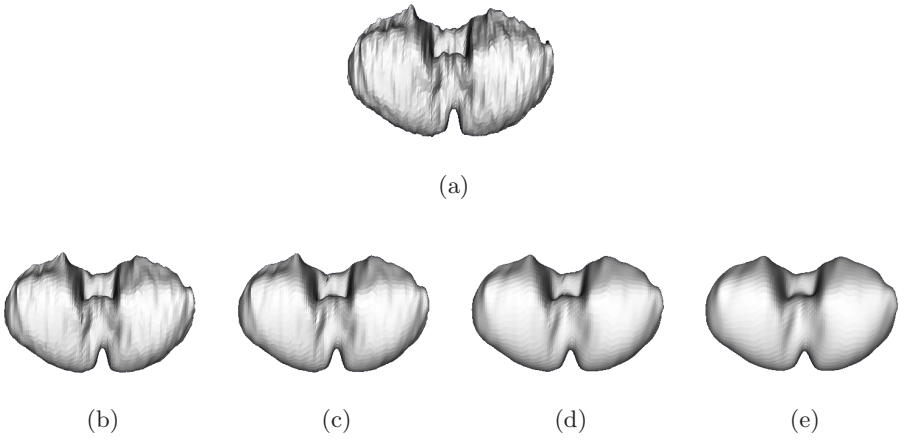

(a) (b) (c) (d) (e)

Fig. 4. Result of applying our deformation model on a cerebellum surface. (a) Initial surface. (b) Iteration 500. (c) Iteration 1000. (d) Iteration 2000. (e) Iteration 3000.

expansion while an increasing J_i, a local area shrinkage. Also, let us define the average area factor as $\bar{J} = 1/N \sum_i^N J_i$ and the normalized area factor as the ratio between the local area factor J_i and the average area factor $\bar{J}$. This factor $J/\bar{J}$ gives an estimation of the local area changes related to the distortion of the total area of the surface.

Results. Figure 3 illustrates the whole process on actual brain stem data. Upper panel (Figure 3(a)) corresponds to the original data and lower Figures 3(b), 3(c), 3(d) and 3(e) stand for the resulting meshes after 500, 1000, 2000, and 3000 iterations, respectively. The deformation method, applied on the brain stem, presented a local area distortion of about a 4% in the 97% of the patches after 3000 iterations. Regarding performance time, image 3(e) is obtained after 223 s, a time which can be considered as adequate for measures in actual morphometrical studies.

Table 1 shows the normalized area factor between the interval $[0, 2]$ for the brain stem surface. A ratio close to one indicates little area changes, that is to say that the local and overall changes are comparable. Figures indicate small changes since most patches present a ratio close to 1.

Table 2. Normalized area factor $J/\bar{J}$ for the cerebellum surface

$J/\bar{J}$	Number of patches	% of patches
$0.0 - 0.75$	0	0 %
$0.76 - 0.95$	12	0.26 %
$0.96 - 1.04$	4622	99.40 %
$1.05 - 1.24$	0	0 %
$1.25 - 2.0$	16	0.34 %

Table 3. CPU time needed to generate the example surfaces

Dataset	Number of points	CPU Time			
		Iteration 500	Iteration 1000	Iteration 2000	Iteration 3000
Brain stem	2800	37 s	74 s	147 s	223 s
Cerebellum	4650	61 s	122 s	244 s	366 s

For the cerebellum mesh, local area distortion is close to 4 % in the 99 % of the patches until iteration 3000. Figure 4 presents images of the surface deformation: upper panel (Figure 4(a)) corresponds to the original data set and lower Figures 4(b), 4(c), 4(d) and 4(e) stand for resulting meshes after 500, 1000, 2000, and 3000 iterations, respectively. Calculation time for 3000 iterations is 366 s. The normalized area factor, as shown in Table 2, is again consistent with little area changes.

Performance analysis. Table 3 summarizes the calculation time required for generating the resulting meshes presented before. It is important to point out that the intermediate meshes obtained after each iteration are not visualized and only the final surface is rendered. As observed in Table 3, CPU performs 8.2 iterations for the cerebellum mesh in one second, while the brain stem surface demands 13.5 iterations for the same time, perfectly compatible with actual clinical practice.

4 Conclusions

We have presented a deformation method which permits to generate smoothed representations of neuroanatomical structures. These structures are represented as surfaces approximated by triangulated meshes, in such a way that these rather simple representations allow us to obtain and efficient and fast deformation under a local area preservation restriction. This approach is efficient because of the little area changes and fast in terms of adequate visualization in actual clinical practice.

Each node velocity is given by a geometrical varying motion field to which area preserving constraints are applied. We use a mixed local-global area preservation constraint to enhance the success of the algorithm. The mathematical structure of the constrained motion model allows us to simply integrate the motion on a per node basis, with no need to solve large systems of equations on

each integration step. Finally, we have shown applicability of this algorithm to compute inflated representations of neuroanatomical structures from real data. Future work includes a parameter analysis for better tuning of the algorithm performance. Also, clinical evaluation of this method is needed in actual morphometrical studies.

References

1. Filippi, M., Horsfield, M., Bressi, S., Martinelli, V., Baratti, C., Reganati, P., Campi, A., Miller, D., Comi, G.: Intra- and inter-observer agreement of brain mri lesion volume measurements in multiple sclerosis. a comparison of techniques. brain 6, 1593–1600 (1995)
2. Tapp, P.D., Head, K., Head, E., Milgram, N.W., Muggenburg, B.A., Su, M.Y.: Application of an automated voxel-based morphometry technique to assess regional gray and white matter brain atrophy in a canine model of aging. NeuroImage 29, 234–244 (2006)
3. Mangin, J., Riviere, D., Cachia, A., Duchesnay, E., Cointepas, Y., Papadopoulos-Orfanos, D., Collins, D., Evans, A., Regis, J.: Object-based morphometry of the cerebral cortex. IEEE Trans Med Imaging 23, 968–982 (2004)
4. Filipek, P.A., Kennedy, D.N., Jr., V.S.C., Rossnick, S.L., Spraggins, T.A., Starewicz, P.M.: Magnetic resonance imaging-based brain morphometry: Development and application to normal subjects. Annals of Neurology 25, 61–67 (1989)
5. Ashtari, M., Zito, J., Gold, B., Lieberman, J., Borenstein, M., Herman, P.: Computerized volume measurement of brain structure. Invest Radiol. 25, 798–805 (1990)
6. Kass, M., Witkin, A., Terzopoulos, D.: Snakes: active contour models. International Journal of Computer Vision 1, 321–331 (1988)
7. Terzopoulos, D., Witkin, A., Kass, M.: Constraints on deformable models: recovering 3D shape and nonrigid motion. Artificial Intelligence 36, 91–123 (1988)
8. Montagnat, J., Delingette, H., Ayache, N.: A review of deformable surfaces: topology, geometry and deformation. Image and Vision Computing 19, 1023–1040 (2001)
9. Carman, G.J., Drury, H.A., Essen, D.C.V.: Computational methods for reconstructing and unfolding the cerebral cortex. cerebral cortex 5, 506–517 (1995)
10. Drury, H., Van Essen, D., Anderson, C., Lee, C., Coogan, T., Lewis, J.: Computarized mappings of the cerebral cortex: a multiresolution flattening method and a surface-based coordinate system. Journal of Cognitive Neuroscience 1, 1–28 (1996)
11. Essen, D.C.V., Drury, H.A.: Structural and functional analyses of human cerebral cortex using a surface-based atlas. The Journal of Neuroscience 17, 7079–7102 (1997)
12. Essen, D.C.V., Drury, H.A., Joshi, S., Miller, M.I.: Functional and structural mapping of human cerebral cortex: Solutions are in the surfaces. Neuroimaging of Human Brain Function 95, 788–795 (1998)
13. Drury, H.A., Corbetta, M., Shulman, G., Essen, D.C.V.: Mapping fMRI activation data onto a cortical atlas using surface-based deformation. NeuroImage 7, S728 (1998)
14. Joshi, M., Cui, J., Doolittle, K., Joshi, S., Essen, D.V., Wang, L., Miller, M.I.: Brain segmentation and the generation of cortical surfaces. NeuroImage 9, 461–476 (1999)
15. Essen, D.C.V., Drury, H.A., Dickson, J., Harwell, J., Hanlon, D., Anderson, C.H.: An integrated software suite for surface-based analyses of cerebral cortex. Journal of the American Medical Informatics Association 8, 443–459 (2001)

16. Harwell, J., Essen, D.V., Hanlon, D., Dickson, J.: Integrated software for surface-based analyses of cerebral cortex. NeuroImage 13, 148 (2001)
17. Fischl, B., Sereno, M.I., Tootell, R.B., Dale, A.M.: High-resolution intersubject averaging and a coordinate system for the cortical surface. Human Brain Mapping 8, 272–284 (1999)
18. Dale, A.M., Fischl, B., Sereno, M.I.: Cortical surface-based analysis I: Segmentation and surface reconstruction. NeuroImage 9, 179–194 (1999)
19. Fischl, B., Sereno, M.I., Dale, A.M.: Cortical surface-based analysis II: Inflation, flattening, and a surface-based coordinate system. NeuroImage 9, 195–207 (1999)
20. Fischl, B., Liu, A., Dale, A.M.: Automated manifold surgery: Constructing geometrically accurate and topologically correct models of the human cerebral cortex. IEEE Transactions on Medical Imaging 20, 70–80 (2001)
21. Angenent, S., Haker, S., Tannenbaum, A., Kikinis, R.: On the Laplace-Beltrami operator and brain surface flattening. IEEE Transactions on Medical Imaging 18, 700–711 (1999)
22. Haker, S., Angenent, S., Tannenbaum, A., Kikinis, R., Sapiro, G., Halle, M.: Conformal surface parameterization for texture mapping. IEEE Transactions on Visualization and Computer Graphics 6, 181–189 (2000)
23. Gu, X., Yau, S.-T.: Computing conformal structure of surfaces. CoRR: Graphics (2002)
24. Hurdal, M.K., Stephenson, K.: Cortical cartography using the discrete conformal approach of circle packings. NeuroImage 23, s119–s128 (2004)
25. Ju, L., Stern, J., Rehm, K., Schaper, K., Hurdal, M., Rottenberg, D.: Cortical surface flattening using least square conformal mapping with minimal metric distortion. 2004 2nd IEEE International Symposium on Biomedical Imaging: Macro to Nano 1, 77–80 (2004)
26. Wang, Y., Gu, X., Chan, T.F., Thompson, P.M., Yau, S.T.: Intrinsic brain surface conformal mapping using a variational method. Proceedings of SPIE - The International Society for Optical Engineering 5370, 241–252 (2004)
27. Hermosillo, G., Faugueras, O., Gomes, J.: Cortex unfolding using level set methods. Technical report, INRIA: Institut National de Recherche en Informatique et en Automatique (1999)
28. Tasdizen, T., Whitaker, R., Burchard, P., Osher, S.: Geometric surface smoothing via anisotropic diffusion of normals. In: 13th IEEE Visualization 2002 (VIS 2002), IEEE Computer Society Press, Los Alamitos (2002)
29. DoCarmo, M.P.: Differential Geometry of Curves and Surfaces. Prentice-Hall, Englewood Cliffs (1976)
30. Pons, J.-P., Keriven, R., Faugeras, O.: Area preserving cortex unfolding. In: Medical Image Computing and Computer-Assisted Intervention MICCAI, Proceedings, pp. 376–383 (2004)
31. Sethian, J.A.: Level Set Methods and Fast Marching Methods: Evolving Interfaces in Computational Geometry, Fluid Mechanics, Computer Vision, and Materials Science. Cambridge University Press, Cambridge (1999)
32. Press, W.H., Teukolsky, S.A., Vetterling, W.T., Flannery, B.P.: Numerical Recipes in C: The Art of Scientific Computing, 2nd edn. Cambridge University Press, Cambridge (1992)